Free evolution vortex in a magnetic field

Zhao-Bo Wang,[1,*] Long Chen,[1,*] Yan-Wu Cao,[2] Chun-Xu Ke,[2] Juan-Cheng Yang,[2] and Ming-Jiu Ni[1,2,†]

[1]*School of Engineering Science, University of Chinese Academy of Sciences, Beijing 101408, People's Republic of China*

[2]*State Key Laboratory for Strength and Vibration of Mechanical Structures, School of Aerospace, Xi'an Jiaotong University, Xi'an 710049, People's Republic of China*

(Received 23 May 2023; accepted 14 August 2023; published 30 August 2023)

The prolonged temporal evolution of a magnetohydrodynamic (MHD) vortex influenced by a steady magnetic field along its axis is investigated both numerically and experimentally within a cubic domain. We directly validate the theory proposed by Davidson [J. Fluid Mech. **299**, 153 (1995)] through numerical analysis: the angular momentum parallel with a magnetic field of a single vortex is conserved, whereas the perpendicular angular momentum decayed exponentially during a free-decay evolution. Moreover, as observed by Sreenivasan and Alboussière [J. Fluid Mech. **464**, 287 (2002)], the initial linear phase, characterized by the dominant influence of the Lorentz force over the inertial force ($N_t \gg 1$, where N_t represents the true interaction parameter), and the subsequent nonlinear phase, marked by an equilibrium between the Lorentz force and the inertial force ($N_t \sim 1$), are successfully corroborated through numerical and experimental means, particularly at a substantial initial interaction parameter ($N_0 > 1$, where N_0 denotes the initial interaction parameter). The transition time from linear phase to nonlinear phase varies with the square of N_0. The relative magnitude of the Lorentz force and the inertial force plays a pivotal role during the free-decay evolution, and we propose the governing equations for such a flow. Nevertheless, numerical simulations and experiments indicate that these two phases and the ensuing transition, as depicted by the velocity decay curve, are primarily limited to the vicinity of the vortex's periphery, exhibiting a certain degree of locality. By considering the scaling of the global kinetic energy [$\sim(t/\tau)^{-0.8}$, where t denotes the physical evolution time normalized by the Joule time τ], the Joule dissipation [$\sim(t/\tau)^{-2}$], and the parallel length [$\sim(t/\tau)^{3/5}$], it becomes evident that the global behavior of a vortex bears greater resemblance to the nonlinear phase rather than undergoing a direct transformation from one phase to another, even when subjected to a substantial initial interaction parameter.

DOI: 10.1103/PhysRevFluids.8.083703

I. INTRODUCTION

Magnetohydrodynamic (MHD) flows exhibit two distinct characteristics that set them apart from conventional flows. First, the presence of a magnetic field causes the flow structures to elongate and align themselves uniformly along the field. Second, the movement of liquid across the magnetic field induces electric currents, resulting in Joule dissipation. Extensive experimental and numerical investigations have observed these properties under the assumption of a low magnetic Reynolds

*These authors contributed equally to this work.
†mjni@ucas.ac.cn

number, denoted as R_m (where $R_m = \mu_m \sigma U_0 L$, with μ_m representing the magnetic permeability of vacuum, σ denoting the electrical conductivity, and U_0 and L_0 being the typical characteristic velocity and length scale, respectively). In the context of $R_m \ll 1$, the induced magnetic field $\boldsymbol{b}$ is significantly smaller than the applied field $\boldsymbol{B}$ ($\boldsymbol{b} \sim R_m \boldsymbol{B} \ll \boldsymbol{B}$), making it a suitable condition for laboratory-scale configurations.

In MHD flows, the presence of Joule dissipation induced by velocity gradients along the magnetic field is known to suppress turbulence intensities in that direction, leading to what is known as quasi-two-dimensional (Q2D) turbulence. Similar to 2D approximation of ocean flow [1], rotation [2], and stratification [3] flow, this phenomenon is characterized by velocity correlation coefficients approaching unity in the direction of the field and an energy spectrum with a slope of -3 in the presence of a strong magnetic field, as observed by Alemany *et al.* [4] and Zikanov *et al.* [5], coinciding with the behavior of two-dimensional turbulence [6,7]. Detailed studies on turbulence under a magnetic field and its dimensionality have been conducted using the Flowcube platform [8–10]. These studies experimentally demonstrated the existence of a cutoff length scale that distinguishes between large Q2D structures and small three-dimensional structures, as well as the presence of inverse and direct energy cascades. However, Eckert *et al.* [11] investigated a sodium channel flow with a transverse magnetic field, and their experimental findings showed a spectral slope that varied from $-5/3$ for low interaction parameters ($N \leqslant 1$) to -4 for high interaction parameters ($N \sim 120$). This continual change in the spectral exponent was partially explained using a helical model proposed by Branover *et al.* [12]. The contradiction between the theoretical explanation for Q2D MHD turbulence and the experimental results indicates the existence of a complex mechanism within MHD turbulent flows.

Given that a turbulent flow field is commonly perceived as a conglomeration of vorticity [13], numerous scholars endeavor to expound upon MHD turbulence through the evolution of a singular flow structure, such as a solitary vortex. This approach offers valuable insight into the characteristics of MHD turbulence. The seminal and nuanced theoretical works by Sommeria and Moreau [14] and Davidson [15] laid the foundation for this field of study. Assuming a substantial interaction parameter ($N \gg 1$) and a high Reynolds Number (Re), indicating the predominance of the Lorentz force over inertial and viscous forces, Sommeria and Moreau [14] revealed that vorticity is transported along the magnetic field via diffusion, while the length scales of the flow structures adhere to a certain relationship

$$l_{\parallel} \sim l_{\perp}(t/\tau)^{1/2}, \tag{1}$$

where $l_{\parallel}$ and $l_{\perp}$ represent the parallel and perpendicular length scales to the magnetic field, respectively. The physical evolution time is denoted as t, while τ stands for the Joule time, defined as $\tau = \rho/\sigma B^2$, which represents the time scale for Joule damping of fluid motion [4]. Here, ρ denotes density, σ refers to electrical conductivity, and B represents the magnetic field strength. It has been demonstrated by Davidson [15] that the Lorentz force is incapable of creating or destroying any angular momentum parallel to the magnetic field in volumes that are infinite or bounded by insulating walls. This discovery carries significant implications, particularly in scenarios where the viscosity force can be neglected (large Re, a state easily achieved in liquid metal flows due to low viscosity coefficients). In such cases, the angular momentum remains conserved during the unrestricted evolution of flow structures. When the magnetic field attains sufficient strength, the flow tends to exhibit quasi-two-dimensional (Q2D) behavior, which arises from the preservation of angular momentum parallel to the field, while the perpendicular components decay exponentially, as proposed by Davidson [16]. However, these phenomena can only be observed and studied through decaying turbulence rather than forced turbulence, as mentioned previously.

Burattini *et al.* [17] conducted a numerical investigation of the decay of initial homogeneous turbulence under an imposed magnetic field by large-eddy simulations. The kinetic energy decay law, $\sim(t/\tau)^{-1/2}$, in the initial linear phase, which was earlier considered by Moffatt [18], and the complex nonlinear decay were discussed in detail. However, the angular momentum is difficult to calculate in homogeneous MHD turbulence. As much as the authors know, the conclusion was only verified through the velocity decay law by an experimental study [19], which focused on the free evolution of a single vortex flow under a vortex-axis magnetic field. According to their findings, after an initial linear phase where the dominance of the Lorentz force over other forces allowed neglect of nonlinear inertial terms, the induced current density resulting from the velocity field diminished until the Lorentz force equaled the nonlinear inertial force in magnitude. The fully decaying stage was described by Sreenivasan and Alboussière [20] through order-of-magnitude analysis. During the initial linear phase, following the concept proposed by Moffatt [18], the decay of kinetic energy followed a $(t/\tau)^{-1/2}$ behavior. By combining this with the evolution equation for length scale Eq. (1) and the conservation equation for angular momentum, the formulas can be expressed as

$$E \sim (t/\tau)^{-1/2}, \quad l_{\parallel} \sim l_{\perp}(t/\tau)^{1/2}, \quad E^{1/2} l_{\perp}^2 l_{\parallel}^{1/2} = \text{constant}, \tag{2}$$

where E is the global kinetic energy. For the nonlinear phase, they considered the balance between the Lorentz force and the inertial force and assumed that the true interaction parameter N_t, indicating the actual ratio of the Lorentz to the inertial forces, remained a constant of order unity

$$N_t \sim \frac{\sigma B^2 l_{\perp}}{\rho u}\left(\frac{l_{\perp}}{l_{\parallel}}\right)^2 = N\left(\frac{l_{\perp}}{l_{\parallel}}\right)^2 \sim 1, \tag{3}$$

where u is the typical velocity of the motion and N is the interaction parameter representing the ratio of the turn-over time of an eddy $(l_{\perp}/u)$ to the Joule time (τ). Furthermore, as for a MHD flow, the decay of the global kinetic energy can be expressed as

$$\frac{dE}{dt} = -\varepsilon - D, \tag{4}$$

where ε and D are the viscous and Joule dissipation, respectively. Sreenivasan and Alboussière [19] argued that the Joule dissipation was dominant over the viscous dissipation so that the latter could be neglected during the whole evolution time and an order-of-magnitude study [20] of energy decay showed that

$$\frac{\varepsilon}{D} \sim \frac{\ln Re(k_0)}{Re(k_0)}, \tag{5}$$

where k_0 is the large (energy-containing) scales. Considering the dominant Joule dissipation over the viscosity dissipation and the parallel angular momentum conservation equation, the formulas for the nonlinear phase can be written as

$$\frac{dE}{dt} \sim -\frac{E}{\tau}\left(\frac{l_{\perp}}{l_{\parallel}}\right)^2, \quad \frac{\sigma B^2 l_{\perp}}{\rho u}\left(\frac{l_{\perp}}{l_{\parallel}}\right)^2 \sim 1, \quad E^{1/2} l_{\perp}^2 l_{\parallel}^{1/2} = \text{constant}. \tag{6}$$

As a result, the evolution of the global kinetic energy E, the perpendicular length scale $l_{\perp}$, the parallel length scale $l_{\parallel}$, along with nondimensional time t/τ could be deduced from Eqs. (2) and (6), respectively, as

$$\begin{aligned} &E/E_0 \sim (t/\tau)^{-1/2}, \quad l_{\perp}/l_0 = \text{constant}, \quad l_{\parallel}/l_0 \sim (t/\tau)^{1/2}, \quad \text{linear phase}, \\ &E/E_0 \sim (t/\tau)^{-1}, \quad l_{\perp}/l_0 \sim (t/\tau)^{1/10}, \quad l_{\parallel}/l_0 \sim (t/\tau)^{3/5}, \quad \text{nonlinear phase}, \end{aligned} \tag{7}$$

and combined with Eq. (3), the transition between the two phases is located at $t = N_0^2\tau$, where the subscript "0" represents the initial state. The experimental validation of these formulas was carried out by Sreenivasan and Alboussière [19] through the measurement of local velocity decay using a five-point-electrode system. This system consisted of four negative electrodes positioned at the corners of a square, with a positive electrode placed at the center. The initial vortex was generated by applying a current pulse through the positive electrode. By considering Eq. (7) and estimating the kinetic energy as $E = \int_V u^2 dV \sim \overline{u^2} l_{\perp}^2 l_{\parallel}$, the average of the squared velocity emerges:

$$\begin{aligned} &\overline{u^2} \sim (t/\tau)^{-1}, \quad \text{linear phase}, \\ &\overline{u^2} \sim (t/\tau)^{-9/5}, \quad \text{nonlinear phase}. \end{aligned} \tag{8}$$

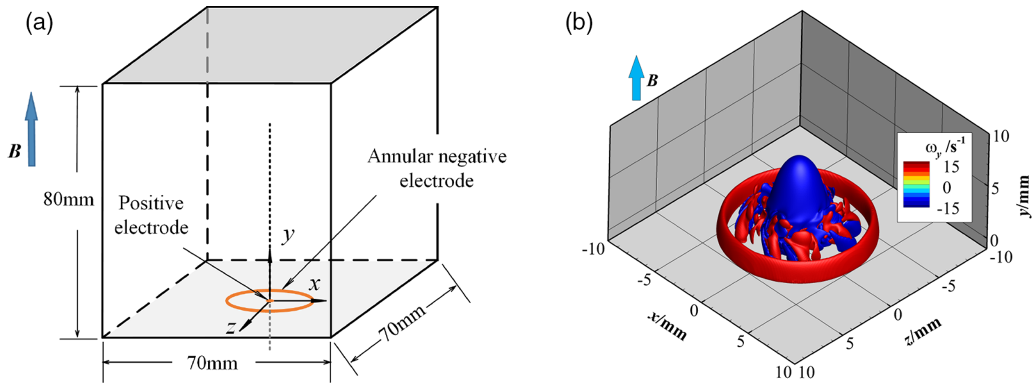

FIG. 1. (a) Geometry of the cubic box with y direction magnetic field. (b) Vorticity field of ω_y at $t = 6\tau$ of $N_0 = 8$.

In the experiment conducted by Sreenivasan and Alboussière [19], the characteristic velocity was measured using wall potential probes positioned at the outer edge of the vortex. While the two scaling laws [Eq. (8)] have been well established, along with Eq. (7) and the verification of parallel angular momentum conservation, there remain several unanswered questions. First, the energy decay equation during the nonlinear phase ($N_t \sim 1$) suggests that Joule dissipation is dominant. Therefore, it is reasonable to expect that this property should hold even better during the linear phase ($N_t > 1$), which contradicts the linear decay law [Eq. (2)]. Second, due to limitations in the experimental measurement method, the evolution of vortex length scale and the total kinetic energy decay in the presence of a magnetic field are still unclear. Furthermore, considering the local velocity measurements in the experiment, a deeper investigation is needed to understand the velocity evolution within the inner region and the laws governing the conservation of parallel angular momentum. These unresolved aspects have motivated the undertaking of numerical simulations to study the detailed evolution of a single vortex. Additionally, a sophisticated experiment has been conducted to further validate the findings of the numerical simulations.

II. PROBLEM STATEMENT AND FORMULATION

A. Governing equations and numerical simulation

The physical model, depicted in Fig. 1(a), consists of a cubic domain with dimensions $x \times y \times z = 70$ mm $\times$ 80 mm $\times$ 70 mm filled with mercury. A current pulse is injected from the positive electrode, located at the center of the bottom wall with a diameter of $d_+ = 1$ mm, and exits the liquid through an annular negative electrode on the bottom. The center of the annular negative electrode coincides with the origin, similar to the positive electrode, with an inner radius of $r_0 = 5$ mm and a width of $d_- = 1$ mm. The properties of mercury are assumed constant (density $\rho = 1.3529 \times 10^4$ kg/m^3, kinematic viscosity $\nu = 1.1257 \times 10^{-7}$ m^2/s, and electrical conductivity $\sigma = 1.055 \times 10^6$ S/m). An external homogeneous magnetic field $\boldsymbol{B}$ is applied along the y direction [$\boldsymbol{B} = (0, B, 0)$]. In the regime of low magnetic Reynolds number (R_m), the governing equations for MHD flows can be expressed as [21]

$$\nabla \cdot \boldsymbol{u} = 0, \tag{9}$$

$$\frac{\partial \boldsymbol{u}}{\partial t} + (\boldsymbol{u} \cdot \nabla)\boldsymbol{u} = -\frac{1}{\rho}\nabla p + \nu \Delta \boldsymbol{u} + \frac{1}{\rho}(\boldsymbol{j} \times \boldsymbol{B}), \tag{10}$$

$$\boldsymbol{j} = \sigma(-\nabla\phi + \boldsymbol{u} \times \boldsymbol{B}), \tag{11}$$

$$\nabla \cdot \boldsymbol{j} = 0, \tag{12}$$

where $\boldsymbol{j}$, ϕ, ν, p, and ρ denote the current density, the electric potential, the kinematic viscosity, the pressure, and the density, respectively.

The injected current interacts with the magnetic field and gives rise to a swirl motion near the bottom. The liquid accelerated by the Lorentz force during the pulse time could be approximatively written as

$$\frac{\partial \boldsymbol{u}}{\partial t} = \frac{1}{\rho}(\boldsymbol{j} \times \boldsymbol{B}). \tag{13}$$

For simplicity, the local cylindrical coordinate (r, θ) is used to describe the local swirl motion of liquid metal, as shown in Fig. 1(b). Thus, after the current pulse, the characteristic swirl velocity can be estimated by integrating the above equation:

$$u_\theta \sim \frac{t_p I B}{\pi r_0^2 \rho}, \tag{14}$$

where t_p represents the duration of the current pulse in seconds, I denotes the injected current, and r_0 corresponds to the inner radius of the annular negative electrode. It is important to note that the chosen value for the current pulse duration, t_p, should be shorter than the Joule time. This ensures that the generation of the vortex does not significantly impact its elongation, as the characteristic time for elongation is determined by the Joule time during the subsequent free decay period. Conversely, excessively small values of t_p would result in a flattened vortex along the bottom wall, preventing the initial vortex (or the vortex formed at the end of the current pulse) from exhibiting three-dimensional characteristics. For instance, when considering a magnetic field strength of 0.6 T acting on mercury, the Joule time is estimated to be approximately 35 ms. Hence, a current pulse duration of $t_p = 10$ ms would be suitable in this case. The Hartmann number Ha, the Reynolds number Re, and the initial interaction parameter N_0 are defined as

$$Ha = Bh\sqrt{\frac{\sigma}{\rho\nu}}, \quad Re = \frac{u_\theta L}{\nu}, \quad N_0 = \frac{\sigma B^2 L}{\rho u_\theta}, \tag{15}$$

where h is the height of the cubic domain, L is the characteristic length of the vortex.

Following the experiment of [19], no-slip conditions for velocity are applied at all walls. As for the electric potential, perfectly insulating conditions are applied on walls except for electrodes on the bottom

$$u = 0, \quad \partial_y \phi = 0. \tag{16}$$

At the positive electrodes on the bottom,

$$\begin{aligned} &u = 0, \quad \partial_y \phi = \frac{I}{S_+ \sigma}, \quad t \leqslant t_p, \\ &u = 0, \quad \partial_y \phi = 0, \quad t > t_p, \end{aligned} \tag{17}$$

TABLE I. Grid details.

Meshes	Grid points in y direction, N_y	Minimum mesh size in y direction, $\Delta y_{\min}/h$	Number of cells in positive electrode	Maximum deviation of $\overline{u}_\theta$ from $G3$
$G1$	300	7.5×10^{-5}	148	1.1%
$G2$	400	3.25×10^{-5}	256	0.05%
$G3$	450	1.6×10^{-5}	256	

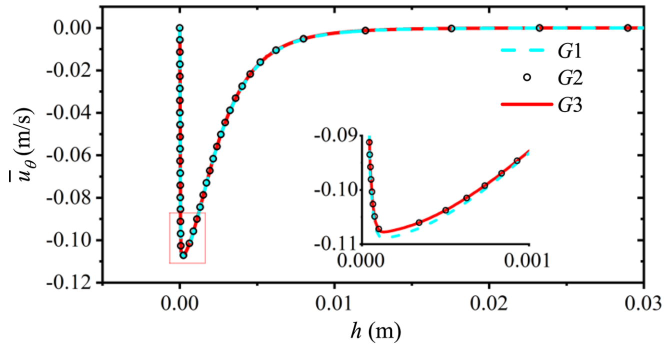

FIG. 2. Grid sensitivity study.

where S_+ is the area of the positive electrodes. And at the annular negative electrodes on the bottom,

$$\begin{aligned} &u = 0, \quad \phi = 0, \quad t \leqslant t_p, \\ &u = 0, \quad \partial_y \phi = 0, \quad t > t_p. \end{aligned} \tag{18}$$

The direct numerical simulations of the governing equation are performed on the finite volume approach based on a consistent and conservative scheme [22]. The detail and the verification of the approach can be referred in Chen *et al.* [23]. Regarding the grid resolution, three variations of meshes are employed in the numerical investigation with $B = 0.8$ T and $N_0 = 5$. As illustrated in Table I and Fig. 2, the grid denoted as $G2$ is adequately refined and surpasses the required level of resolution for our particular problems.

B. Experimental setup and procedure

Experiments are conducted within a cylindrical enclosure characterized by electrically insulating boundaries and subject to a vertical magnetic field, as depicted in Fig. 3. The enclosure, possessing an inner diameter of $D = 70$ mm and a height of $h = 80$ mm, is filled with gallium-indium-tin eutectic (GaInSn). Similar to the numerical simulation, the liquid is propelled by a current pulse, which is introduced through a positively charged central electrode (with a diameter of $d_+ = 1$ mm)

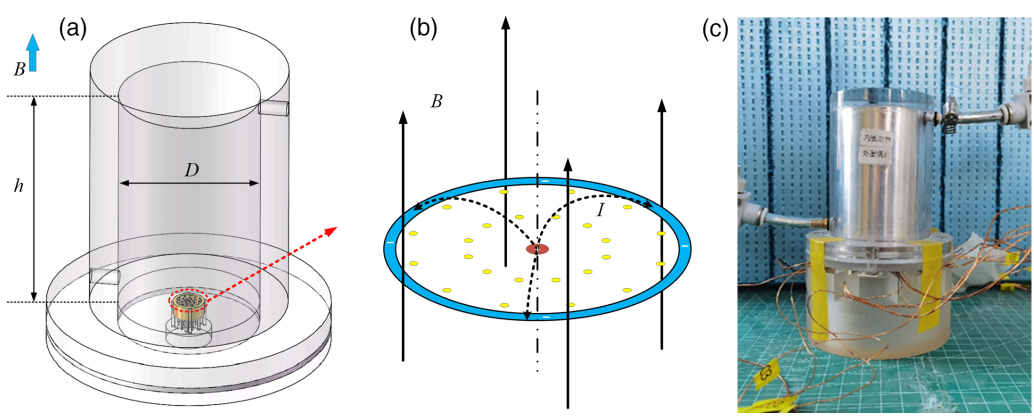

FIG. 3. (a) Sketch of the experiment set up ($D = 70$ mm, $h = 80$ mm). (b) Details of the point positive electrode (red), the annular negative electrode (blue), and the wall potential probes (yellow) on the bottom. (c) The cylindrical cavity filled with GaInSn.

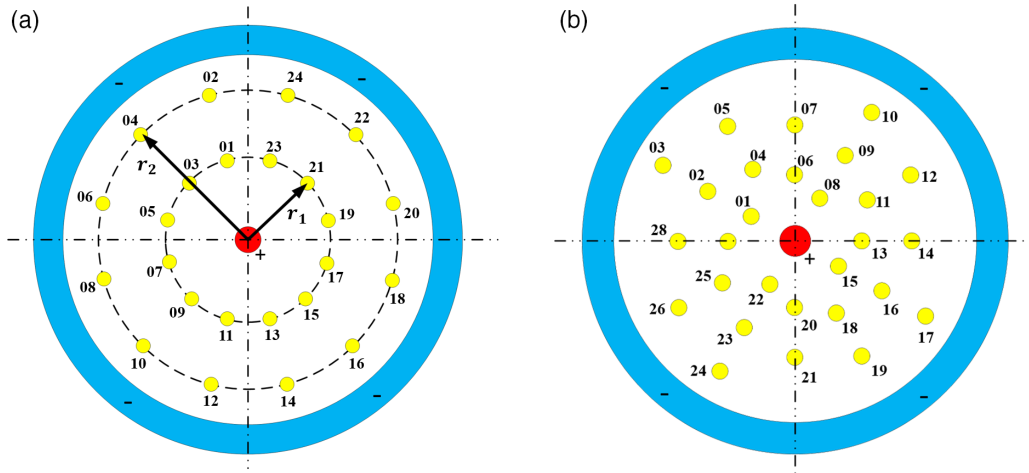

FIG. 4. Different types of wall potential probes arrangement and the position information of the probes can be referred to Table II. (a) Type A for measuring velocity decay at the outer edge of the vortex. (b) Type B for measuring the global velocity decay.

and exits the liquid via a ring-shaped negative electrode (with an inner radius of $r_0 = 5$ mm and a width of $d_- = 1$ mm) located at the bottom.

Velocity is locally measured using multiple wall potential probes positioned on the bottom, a widely employed technique in MHD flows [19,24]. In Fig. 4, two different configurations of potential probes are utilized to assess the velocity decay at the outer periphery of the vortex (Type A) and the global evolution of the vortex (Type B). For Type A, twelve pairs of probes are uniformly distributed azimuthally from $r_1 = 2.5$ mm to $r_2 = 4.5$ mm, with a spacing of 2 mm between each pair. Here, r_1 and r_2 denote the radial positions for a single pair of probes. In the case of Type B, four sets of potential probes with varying radial positions ($r_1 = 1.5, 2.0, 2.5, 3.0$ mm, $r_2 = r_1 + 1.5$) are employed to measure the velocity at different radii, and the average value among them signifies the global velocity evolution. All potential signals are recorded at a sampling rate of 500 Hz. By subtracting background noise and averaging the signals over eight repetitions, reliable results are obtained. For detailed information regarding the measurement scheme and probe positions, please refer to Table II.

III. RESULTS AND DISCUSSION

Table III lists the initial conditions and the dimensional groups of simulations.

TABLE II. Position information of the wall potential probes.

	Probs position r_1–r_2/mm	Number of measuring points
Type A	2.5–4.5	01–02, 03–04, 05–06, 07–08, 09–10, 11–12, 13–14, 15–16, 17–18, 19–20, 21–22, 23–24
Type B	1.5–3.0	01–02, 08–09, 15–16, 22–23
	2.0–3.5	06–07, 13–14, 20–21, 27–28
	2.5–4.0	04–05, 11–12, 18–19, 25–26
	3.0–4.5	02–03, 09–10, 16–17, 23–24

TABLE III. Simulated cases.

B(T)	τ(s)	t_p(s)	I(A)	Re	N_0	Ha
0.8	0.0200	0.01	13.33	8915	5.0	1684
0.8	0.0200	0.01	9.50	6354	7.0	1684
0.8	0.0200	0.01	7.30	4882	9.0	1684
0.75	0.0228	0.01	7.75	4859	8.0	1579
0.65	0.0304	0.01	13.4	7281	4.0	1368
0.6	0.0356	0.01	8.20	4113	6.0	1263
0.6	0.0356	0.01	20.0	10032	2.5	1263

A. The evolution of angular momentum

Davidson [15] initially postulated that the angular momentum $\boldsymbol{H} = \int_V \boldsymbol{x} \times \boldsymbol{u} dV$ of a vortex decaying in the presence of an axial magnetic field undergoes evolution according to the following equation:

$$H_{\parallel} = \text{constant}, \quad H_{\perp} = H_{\perp}(0)e^{-t/4\tau} \tag{19}$$

in the direction parallel and perpendicular to the field, respectively, based on the assumption of inviscid flow. Owing to the viscosity of the liquid metal and the no-slip Hartmann wall, there exists a disparity between the theoretical prediction, Eq. (19), and the outcomes of our simulations. Figure 5 illustrates the simulated decay process of both the perpendicular and parallel angular momentum. During the current pulse, the Lorentz force generated by the electric current impels the rotation of the liquid metal around the positive electrode, while the fluid motion is propelled away from the bottom wall under the influence of viscosity and the magnetic field. As the driving force predominates during this period, the initial flow structure is established in a three-dimensional manner. As depicted in Fig. 5(a), the perpendicular angular momentum, denoted as $H_{\perp}$, when normalized by the value at the termination of the current pulse, exhibits satisfactory agreement across various initial interaction parameters N_0. Furthermore, a commendable concurrence is observed between the numerical findings presented here and the fitting curve

$$\frac{H_{\perp}}{H_{\perp}(0)} = 1.2e^{-t/4\tau}, \tag{20}$$

indicating an exponential decay of $H_{\perp}$ and corresponding well with the theory of Davidson [15]. On the other hand, as shown in Fig. 5(b), the parallel angular momentum $H_{\parallel}$ decays nearly linearly

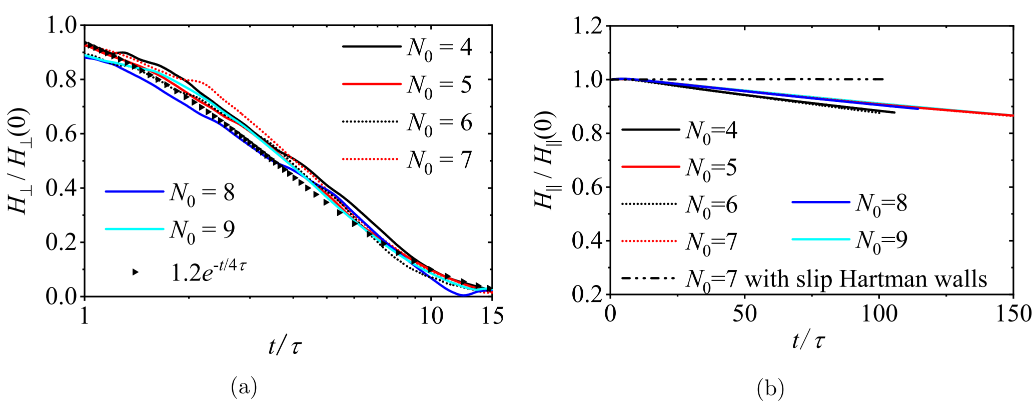

FIG. 5. Time evolution of parallel and perpendicular angular momentum.

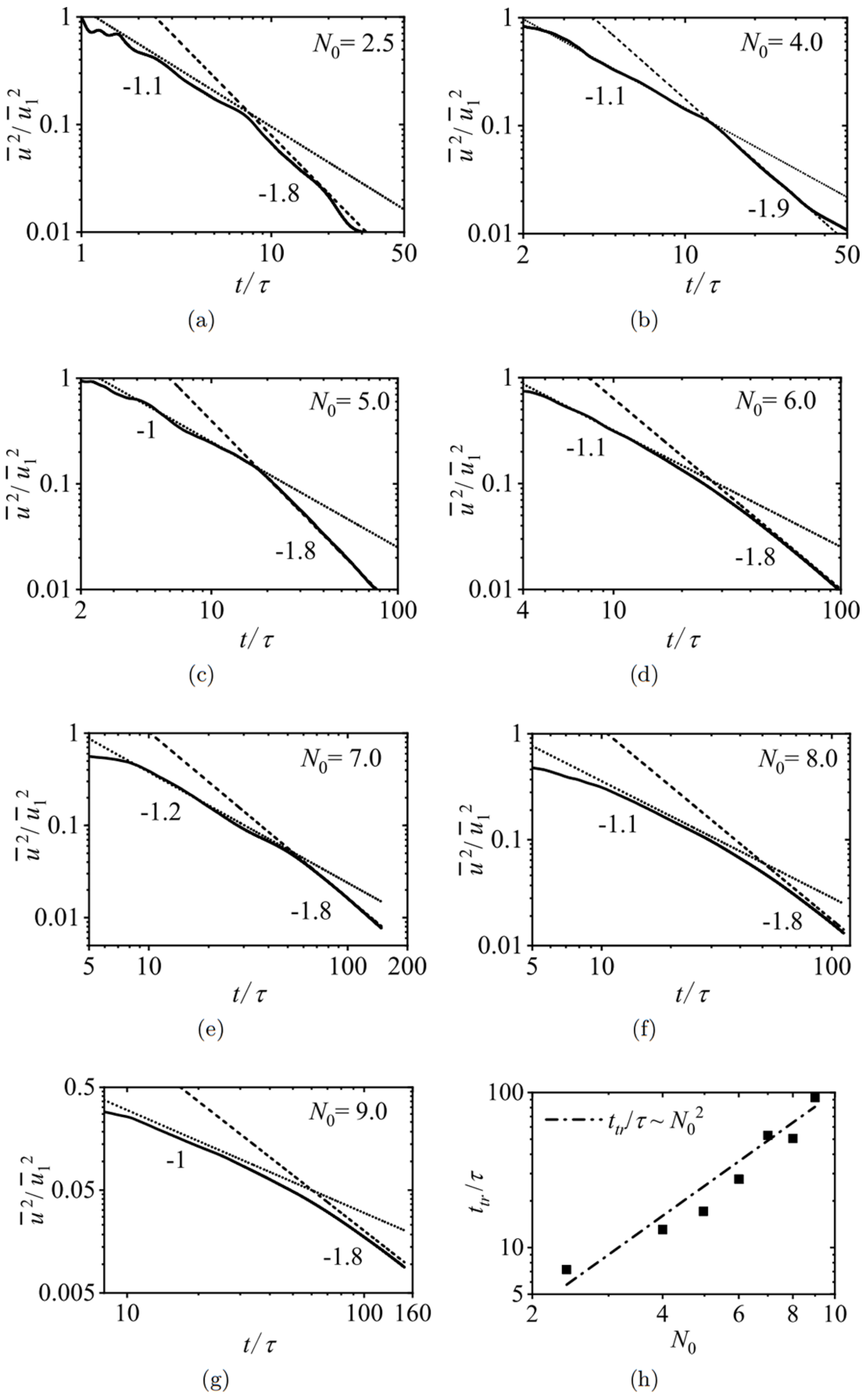

FIG. 6. Time evolution of mean square velocity (a $\sim$ g), linear-nonlinear transition time (h) for numerical simulations.

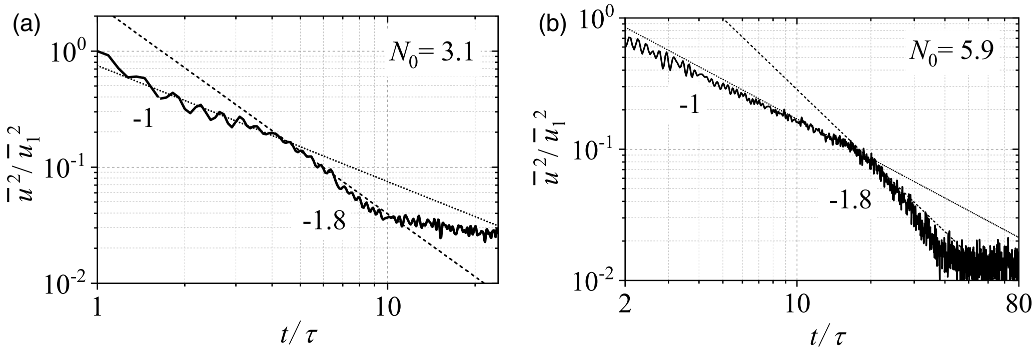

FIG. 7. Experiment measure for mean square velocity as a function of time. (a) $N_0 = 3.1$, $B = 0.4$ T. (b) $N_0 = 5.9$, $B = 0.5$ T.

during the whole evolution ($\sim 10^2\tau$) with a decrease of 15%. Compared with the decay time of perpendicular angular momentum ($\sim 10\tau$), it can be concluded that the parallel momentum is conserved during vortex decay. Besides, from the result of slip Hartmann wall configuration, the parallel angular momentum decreases less than 1%. So in our simulation cases, the Hartmann friction near the bottom wall is mainly responsible for the slight decrease of $H_\parallel$. In a more general sense, regarding the evolution of vortices in the bulk region under the influence of a magnetic field, the conservation of parallel angular momentum is expected.

B. Linear and nonlinear phase

One of the noteworthy conclusions drawn by Sreenivasan and Alboussière [19] is the indirect demonstration of Eq. (7), supported by the observation of two distinct phases, namely the linear and nonlinear phases, in the velocity decay curve. However, due to limitations in the measurement method, the velocity information is only collected at the outer edge of the central vortex. Additionally, the center vortex is unavoidably influenced by the vorticity accumulated around the negative electrodes, leading to physical fluctuations as reported in Sreenivasan and Alboussière [19]. Nonetheless, such issues are effectively addressed in our annular negative electrode configuration. Similar to the experiment, local velocity is measured by assessing the potential difference on the bottom wall at the outer edge of the vortex ($r/r_0 \in [0.8, 0.9]$) in each case. To ensure reliable results, the square of velocity u^2 is averaged over forty samples in the θ direction. Normalized by the average value at $t = \tau$ (denoted as $\overline{u_1^2}$), Fig. 6 depicts the decay processes under various initial conditions. The linear phase, characterized by a slope of approximately -1, and the nonlinear phase, characterized by a slope of approximately -1.8, are confirmed and align with our experimental findings using the Type A wall potential probes arrangement (Fig. 7). Furthermore, the transition time t_{tr} between these two phases exhibits a good fit with the curve $t_{tr}/\tau \sim N_0^2$, as demonstrated in Fig. 6(h).

C. Single-phase scaling laws for the global evolution

1. Elongating effect of Lorentz force

The conservation of $H_\parallel$, coupled with ongoing Joule dissipation, leads to the elongation of eddies along the magnetic field. The ratio between the parallel length scale $l_\parallel$ and the spatial extent in the direction of the magnetic field h plays a crucial role in determining the dimensionality of turbulence [9,10]. In our configuration, the vortex is generated on the bottom wall during the current pulse and subsequently spreads upward under the influence of viscosity and the magnetic field. Figure 8(a) illustrates the evolution of u_θ at different y positions, specifically at $r/r_0 = 0.75$. It can be observed

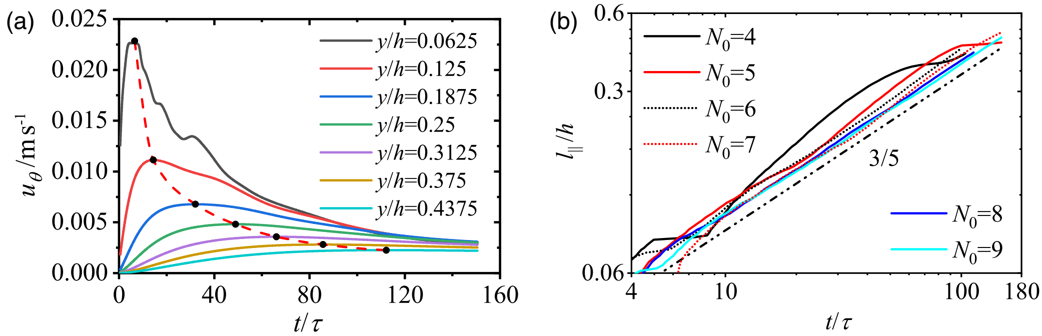

FIG. 8. Velocity evolution at different y/h (a) and evolution of the parallel length scale (b) for $N_0 = 7$ of numerical simulations.

that the liquid metal undergoes acceleration by the underlying fluid, reaching a maximum velocity before gradually decelerating. The relationship between y and the time location of these maxima, indicated by black data points in Fig. 8(a), reflects the time evolution of the parallel length scales for $N_0 = 7$. Figure 8(b) depicts this relationship between the parallel length $l_\parallel$ and time, obtained from the average u_θ at $r/r_0 = 0.75$. With the exception of the initial few Joule times, $l_\parallel$ exhibits a slope of 3/5 throughout the entire simulation, particularly at larger initial interaction parameter N_0, which aligns well with the nonlinear phase decay described in Eq. (7) [19]. It is reasonable for a deviation to occur when the initial interaction parameter is small, such as $N_0 = 4$, as the forcing is strong initially and the Lorentz force does not dominate in such a scenario. Furthermore, it appears that the linear phase, characterized by a growth rate of $l_\parallel/l_0 \sim (t/\tau)^{1/2}$, is not observed during the entire decay process, nor is there a clear transition between the linear and nonlinear decay phases. Additionally, it is worth noting that similar results can be obtained from velocity data at $r/r_0 = 0.6$ and $r/r_0 = 0.9$, indicating that the elongation of a vortex tends to be a nonlinear process. Moreover, Fig. 8 demonstrates that the parallel length scale $l_\parallel/h$ hardly reaches unity even after a long evolution period ($\sim 10^2\tau$). In other words, the fluid near the top wall is consistently accelerated by the underlying liquid metal, and a Q2D state is not achieved by the end of the evolution. This finding is further supported by the velocity profile along the z direction, which exhibits a velocity gradient, contrasting with the results obtained using a velocity correlation coefficient in Sreenivasan and Alboussière [19].

2. *Joule dissipation and energy decay*

Sreenivasan and Alboussière [19] attempted to close the governing equations for the nonlinear phase by considering the dominance of Joule dissipation over viscous dissipation, allowing the neglect of the latter during the evolution time. The ratio between these dissipation terms is expressed in Eq. (5). However, it should be noted that this estimation appears to be inadequate for the nonlinear phase. In line with the approach proposed by Davidson [25], an alternative estimation for the viscous dissipation can be derived as follows:

$$\varepsilon \sim \alpha \frac{u^3}{l_\perp}, \tag{21}$$

where α is a coefficient of order unity. On the other hand, the Joule dissipation can be estimated as

$$D = \frac{1}{\rho\sigma} \int_V \boldsymbol{j}^2 dV. \tag{22}$$

From Ohm's law,

$$\nabla \times \boldsymbol{j} = \sigma \nabla \times (\boldsymbol{u} \times \boldsymbol{B}) = \sigma (\boldsymbol{B} \cdot \nabla)\boldsymbol{u}. \tag{23}$$

When the imposed magnetic field is uniform, the current can be estimated as

$$j \sim \sigma B u \left(\frac{l_\perp}{l_\parallel}\right). \tag{24}$$

Hence, the Joule dissipation can be derived as

$$D = \beta \frac{\sigma B^2}{\rho}\left(\frac{l_\perp}{l_\parallel}\right)^2 \int_V u^2 dV = \beta \frac{E}{\tau}\left(\frac{l_\perp}{l_\parallel}\right)^2, \tag{25}$$

where β is a coefficient of order unity. When the two terms, Eqs. (21) and (25) are in the same order, a simple order-of-magnitude study can be conducted as

$$\frac{u^3}{l_\perp} \sim \frac{u^2}{\tau}\left(\frac{l_\perp}{l_\parallel}\right)^2. \tag{26}$$

It can be easily concluded that the true interaction parameter is on order of unity, $N_t \sim 1$. Such a result is very interesting since it states that the Joule dissipation will fall into the same magnitude with the viscous dissipation at $N_t \sim 1$. Such a state in which the viscous and Joule dissipation are nearly equal after the initial linear phase is also discovered in decay of homogeneous MHD turbulence [17]. Therefore, by combining Eqs. (4) and (25), the energy decay equation should be corrected as

$$\frac{dE}{dt} = -2\beta \frac{E}{\tau}\left(\frac{l_\perp}{l_\parallel}\right)^2, \tag{27}$$

and the angular momentum conservation

$$E^{1/2} l_\perp^2 l_\parallel^{1/2} = \text{constant}. \tag{28}$$

To close the system, we follow Davidson [25] and introduce the equation

$$\frac{d}{dt}(l_\parallel / l_\perp)^2 = 2\beta/\tau, \tag{29}$$

which is a reasonable approximation not only for $N \to 0$ and $N \to \infty$ but also for intermediate N. Additionally, the direct numerical simulation (DNS) conducted by Okamoto *et al.* [26] provides further support for this estimation. Finally, by integrating Eqs. (27), (28), and (29), we obtain the decay laws as follows:

$$E/E_0 = \hat{t}^{-1}, \quad l_\perp / l_0 = \hat{t}^{1/10}, \quad l_\parallel / l_0 = \hat{t}^{3/5}, \tag{30}$$

where $\hat{t} = 1 + 2(t/\tau)$. The derived expressions are consistent with the findings of the nonlinear phase in Sreenivasan and Alboussière [19], and they further support the conclusion that the true interaction parameter is on the order of unity, i.e., $N_t \sim 1$.

During the linear phase, it is reasonable to assume that Joule dissipation dominates when N_0 is sufficiently large. In such cases, the energy decay equation can be expressed as follows:

$$\frac{dE}{dt} = -\beta \frac{E}{\tau}\left(\frac{l_\perp}{l_\parallel}\right)^2. \tag{31}$$

Integrating Eqs. (31), (28), and (29) yields the decay laws

$$E/E_0 = \hat{t}^{-1/2}, \quad l_\perp / l_0 = \text{constant}, \quad l_\parallel / l_0 = \hat{t}^{1/2}. \tag{32}$$

Combined with Eqs. (30) and (32), the scaling of the Joule dissipation can be expressed as

$$\begin{aligned} D/D_0 &\sim \hat{t}^{-3/2}, \quad \text{linear phase} \\ D/D_0 &\sim \hat{t}^{-2}, \quad \text{nonlinear phase}. \end{aligned} \tag{33}$$

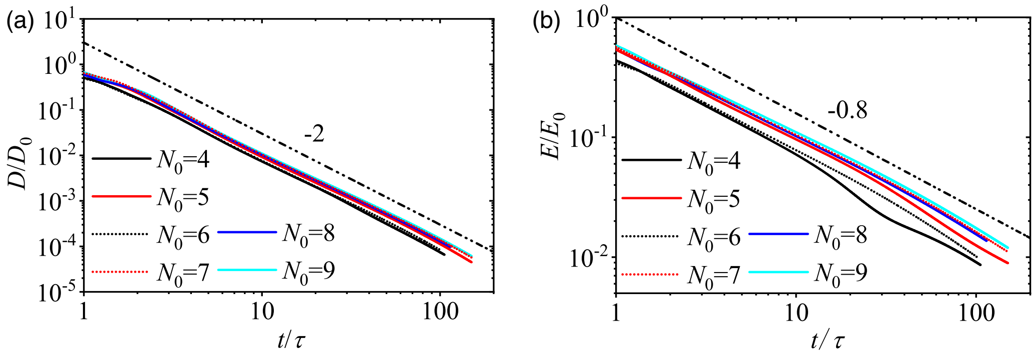

FIG. 9. Time evolution of Joule dissipation and kinetic energy for numerical simulations, normalized by the value at the end of the current pulse, respectively.

Figure 9 shows the time evolution of Joule dissipation, $D = \frac{1}{\rho\sigma}\int_V \boldsymbol{j}^2 dV$, and kinetic energy, $E = \int_V u^2 dV$, in different cases, holding a slope of -2 and -0.8, respectively. For the Joule dissipation, shown in Fig. 9(a), the global integration of Joule dissipation agrees well with the decay law for nonlinear phase [Eq. (33)], indicating the global nonlinear behavior of the vortex evolution. Whereas for the kinetic energy, shown in Fig. 9(b), approximately decays with a scale $(t/\tau)^{-0.8}$. However, only one slope is displayed in each case and no transition exists from the linear phase to the nonlinear phase. Combining with evolution of the Joule dissipation and the parallel scale, we consider the global evolution of the vortex as a nonlinear process.

The global evolution of Joule dissipation and energy appears to deviate from the findings depicted in Fig. 6, which prompts a more detailed investigation. We examine the average velocity, determined by the potential difference between $r/r_0 = 0.5$ and $r/r_0 = 0.6$, as depicted in Fig. 10 for varying values of N_0. Notably, the velocity decay exhibits a consistent slope of approximately ~ -1.6 across all cases, regardless of the initial interaction parameter. It is worth mentioning that this velocity scale (~ -1.6) corresponds with the global energy scale (~ -0.8) governed by $E \sim u^2 l_\perp^2 l_\parallel$ under the assumption of nonlinear evolution of parallel and perpendicular length, as demonstrated in Eq. (30).

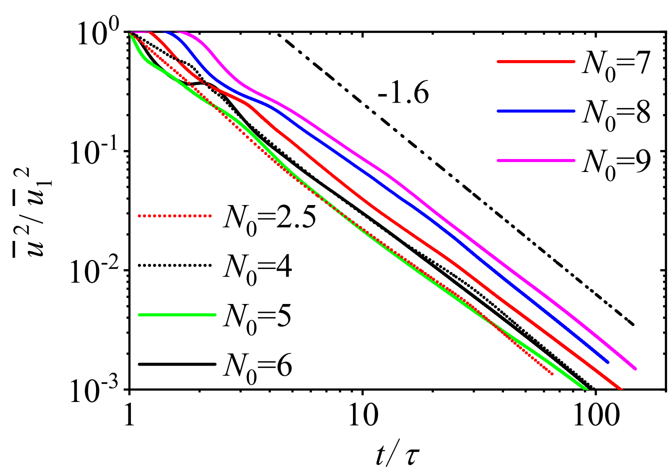

FIG. 10. Velocity decay in inner space for numerical simulations (average velocity between $r/r_0 \in [0.5, 0.6]$).

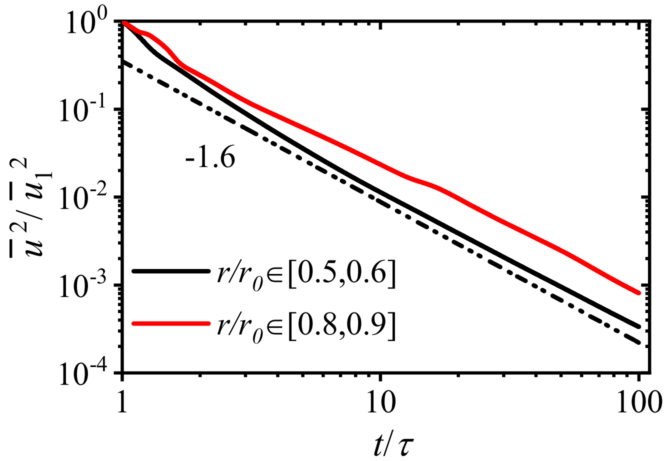

FIG. 11. Velocity decay at different location with $N_0 \sim 1$ for numerical simulations.

Moreover, when focusing on small initial interaction parameters ($N_0 \sim 1$) as depicted in Fig. 11, the decay of velocity in different regions (inner space and outer space of the central vortex) both exhibit a consistent scaling of $t^{-1.6}$ with the disappearance of the transition between the two phases. Notably, for a small interaction parameter, such as $N_0 = 0.7$ observed in the experiment conducted by Sreenivasan and Alboussière [19], only a scaling of $t^{-1.5}$ is observed, which coincides with our findings in the inner space of the vortex. Regarding the velocity decay in the inner space, Eqs. (14) and (15) indicate that the initial interaction parameter satisfies $N_0 \sim L^3$, where L represents the size of circular motion. Therefore, it is the smaller rotational radius that causes the velocity decay in the inner space of a vortex to correspond to fluid motion with a significantly smaller N_0. Such nonuniform decay gives rise to the nonlinear evolution of global kinetic energy, parallel length scale, and Joule dissipation at larger N_0.

To further validate the results, the experimental global velocity evolution is presented in Fig. 12. The signals are averaged across various potential probes positioned at different radii (Type B), as illustrated in Fig. 4(b). For different values of N_0, the decay of mean square velocity follows a

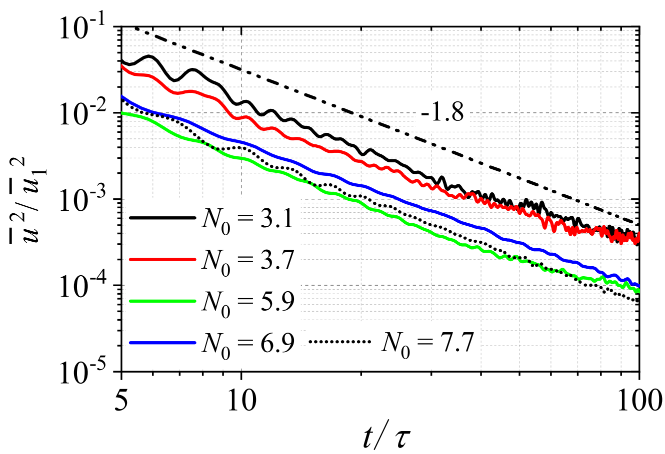

FIG. 12. Experimental measure for global velocity decay in different N_0. Each curve is averaged from all potential probes in Type B.

scaling of $(t/\tau)^{-1.8}$, which aligns with our numerical findings (Fig. 9) and suggests a nonlinear phase in the global evolution.

IV. CONCLUSION

This paper focuses on the numerical and experimental investigation of the free decay of a solitary vortex in a uniform axial-directional magnetic field. The numerical results strongly support the exponential decay of perpendicular angular momentum ($H_\perp \sim H_\perp(0)e^{-t/4\tau}$) and the conservation of parallel angular momentum ($H_\parallel = \text{constant}$). Regarding the elongation of the flow structure in the presence of a magnetic field, the parallel length scale evolves as $l_\parallel \sim (t/\tau)^{3/5}$ for large values of N_0. Numerical simulations, together with the observed Joule dissipation ($\sim(t/\tau)^{-2}$) and global kinetic energy ($\sim(t/\tau)^{-0.8}$), suggest that the global decay of the vortex can be characterized as a nonlinear phase, even when the initial interaction parameter is sufficiently large. This finding is further validated through our experimental findings. Furthermore, the outer edge of the vortex confirms the existence of linear and nonlinear phases, as well as a transition region ($t_{tr} \sim N_0^2\tau$) between them. However, the decay in the inner space of the vortex exhibits a consistent slope throughout the entire evolution, which may contribute to the global nonlinear behavior observed in the decay of a solitary vortex.

The significant work by Sreenivasan and Alboussière [19] introduced a vortex formation technique using the interaction between a magnetic field and an injected current, providing a comprehensive dynamic evolution model under an applied magnetic field. However, it should be noted that this evolution is contingent upon the rotational radius of the fluid, resulting in a discrepancy between the velocity decay at the outer edge and the inner region of the vortex. In terms of global energy evolution, the vortex consistently exhibits a nonlinear phase. These findings contribute to a better understanding of MHD turbulent flows in a broader context.

ACKNOWLEDGMENTS

The authors acknowledge support from MOST under Grant No. 2022YFE03130000 and NSFC under Grants No. 51927812 and No. 52076204.

[1] S. Matle, A 2d numerical ocean model on the coriolis and wind stress effects using stochastics, Theor. Appl. Mech. Lett. **11**, 100282 (2021).

[2] T. Li, M. Wan, and S. Chen, Flow structures, nonlinear inertial waves and energy transfer in rotating spheres, Theor. Appl. Mech. Lett. **11**, 100312 (2021).

[3] J. Paret, D. Marteau, O. Paireau, and P. Tabeling, Are flows electromagnetically forced in thin stratified layers two dimensional?, Phys. Fluids **9**, 3102 (1997).

[4] A. Alemany, R. Moreau, P. Sulem, and U. Frisch, Influence of an external magnetic field on homogeneous MHD turbulence, J. Mec. **18**, 277 (1979).

[5] O. Zikanov, D. Krasnov, T. Boeck, and S. Sukoriansky, Decay of turbulence in a liquid metal duct flow with transverse magnetic field, J. Fluid Mech. **867**, 661 (2019).

[6] R. H. Kraichnan, Inertial ranges in two-dimensional turbulence, Phys. Fluids **10**, 1417 (1967).

[7] G. K. Batchelor, Computation of the energy spectrum in homogeneous two-dimensional turbulence, Phys. Fluids **12**, II-233 (1969).

[8] R. Klein and A. Pothérat, Appearance of Three Dimensionality in Wall-Bounded MHD Flows, Phys. Rev. Lett. **104**, 034502 (2010).

[9] A. Pothérat and R. Klein, Why, how and when mhd turbulence at low becomes three-dimensional, J. Fluid Mech. **761**, 168 (2014).

[10] N. T. Baker, A. Pothérat, L. Davoust, and F. Debray, Inverse and Direct Energy Cascades in Three-Dimensional Magnetohydrodynamic Turbulence at Low Magnetic Reynolds Number, Phys. Rev. Lett. **120**, 224502 (2018).

[11] S. Eckert, G. Gerbeth, W. Witke, and H. Langenbrunner, Mhd turbulence measurements in a sodium channel flow exposed to a transverse magnetic field, Int. J. Heat Fluid Flow **22**, 358 (2001).

[12] H. Branover, A. Eidelman, E. Golbraikh, and S. Moiseyev, *Turbulence and Structures: Chaos, Fluctuations, and Helical Self-Organization in Nature and the Laboratory* (Academic Press, San Diego, 1999).

[13] P. A. Davidson, *Turbulence: An Introduction for Scientists and Engineers* (Oxford University Press, New York, 2015).

[14] J. Sommeria and R. Moreau, Why, how, and when, MHD turbulence becomes two-dimensional, J. Fluid Mech. **118**, 507 (1982).

[15] P. Davidson, Magnetic damping of jets and vortices, J. Fluid Mech. **299**, 153 (1995).

[16] P. Davidson, The role of angular momentum in the magnetic damping of turbulence, J. Fluid Mech. **336**, 123 (1997).

[17] P. Burattini, O. Zikanov, and B. Knaepen, Decay of magnetohydrodynamic turbulence at low magnetic reynolds number, J. Fluid Mech. **657**, 502 (2010).

[18] H. Moffatt, On the suppression of turbulence by a uniform magnetic field, J. Fluid Mech. **28**, 571 (1967).

[19] B. Sreenivasan and T. Alboussière, Experimental study of a vortex in a magnetic field, J. Fluid Mech. **464**, 287 (2002).

[20] B. Sreenivasan and T. Alboussière, Evolution of a vortex in a magnetic field, Eur. J. Mech. B Fluids **19**, 403 (2000).

[21] P. H. Roberts, *An Introduction to Magnetohydrodynamics*, Vol. 6 (Longmans London, London, 1967).

[22] M.-J. Ni, R. Munipalli, P. Huang, N. B. Morley, and M. A. Abdou, A current density conservative scheme for incompressible mhd flows at a low magnetic reynolds number. Part II: On an arbitrary collocated mesh, J. Comput. Phys. **227**, 205 (2007).

[23] L. Chen, A. Pothérat, M.-J. Ni, and R. Moreau, Direct numerical simulation of quasi-two-dimensional mhd turbulent shear flows, J. Fluid Mech. **915**, A130 (2021).

[24] K. Messadek and R. Moreau, An experimental investigation of mhd quasi-two-dimensional turbulent shear flows, J. Fluid Mech. **456**, 137 (2002).

[25] P. Davidson, The role of angular momentum conservation in homogeneous turbulence, J. Fluid Mech. **632**, 329 (2009).

[26] N. Okamoto, P. Davidson, and Y. Kaneda, On the decay of low-magnetic-reynolds-number turbulence in an imposed magnetic field, J. Fluid Mech. **651**, 295 (2010).